Biochimica et Biophysica Acta 1858 (2016) 2539–2548

Contents lists available at ScienceDirect

Biochimica et Biophysica Acta

journal homepage: www.elsevier.com/locate/bbamem

Sampling errors in free energy simulations of small molecules in lipid bilayers☆

Chris Neale [a], Régis Pomès [b,c,*]

[a] Department of Physics, Applied Physics and Astronomy, Rensselaer Polytechnic Institute, 110 8th St, Troy, New York 12180-3590, USA
[b] Molecular Structure and Function, The Hospital for Sick Children, 686 Bay Street, Toronto, Ontario M5G 0A4, Canada
[c] Department of Biochemistry, University of Toronto, 101 College Street, Toronto, Ontario M5G 1L7, Canada

ARTICLE INFO

Article history:
Received 17 December 2015
Received in revised form 1 March 2016
Accepted 2 March 2016
Available online 4 March 2016

Keywords:
Simulation
Free energy
Potential of mean force
Hidden barrier
Orthogonal barrier
Review

ABSTRACT

Free energy simulations are a powerful tool for evaluating the interactions of molecular solutes with lipid bilayers as mimetics of cellular membranes. However, these simulations are frequently hindered by systematic sampling errors. This review highlights recent progress in computing free energy profiles for inserting molecular solutes into lipid bilayers. Particular emphasis is placed on a systematic analysis of the free energy profiles, identifying the sources of sampling errors that reduce computational efficiency, and highlighting methodological advances that may alleviate sampling deficiencies. This article is part of a Special Issue entitled: Biosimulations edited by Ilpo Vattulainen and Tomasz Róg.

1. Introduction

Cells are surrounded and compartmentalized by membranes [1,2]. The main structural components of these membranes are amphipathic phospholipids that form planar bilayers in water [3–5]. The resulting lipophilic core, together with embedded proteins, provides cells and many organelles with selective permeability [6–9], thereby enabling life as we know it. These membranes are so prevalent that even though they are generally only ~5 nm thick [10–12], their constituent lipids comprise ~10% of a cell's dry weight [13–15]. The great biological and biomedical relevance of membrane penetration by molecules such as water [16,17], peptides [18], anesthetics [19], and other drugs [20,21] motivates the study of solute interactions with lipid bilayers and underscores the need for reliable methods to measure and predict the partition free energy of these solutes in membranes.

This review focuses on molecular simulation studies of the partitioning of small molecules between water and the different microenvironments provided by lipid bilayers. Although molecular simulations provide exceptional spatial and temporal resolution, they are only useful when their resulting estimates are both accurate and precise. Errors may arise both from insufficient sampling of thermally-accessible arrangements or conformations of the molecular system of interest (sampling errors) and from inaccuracies in the potential energy functions used to compute molecular interactions (force field errors). Here, we review recent progress in understanding the sampling errors that can occur in simulations aimed at obtaining quantitative estimates of the free energy profile or potential of mean force (PMF) for the insertion of a molecular solute into a lipid bilayer (hereafter referred to as a bilayer PMF). Unless otherwise noted, we limit our investigation to atomistic models. For clarity and brevity we focus on small solutes and generally neglect the numerous simulations aimed at characterizing the interactions between bilayers and relatively large molecules such as proteins, peptides, nucleic acids, polymers [22], and nanoparticles. Furthermore, we focus on computational studies in which the potential energy function is rationally modified to enhance sampling of unlikely but important states by employing methods such as umbrella sampling (US) [23,24] and metadynamics [25] (i.e., importance sampling or free energy simulations) and do not discuss the standard, brute force simulations that can also be used to obtain bilayer PMFs when the relevant sampling barriers are sufficiently small [26,27].

Recent reviews of methods available for computing free energies were provided by Chipot [28], Gumbart et al. [29], and Hansen & van Gunsteren [30]; a review of molecular simulations of lipid bilayers

Abbreviations: PMF, Potential of mean force; US, Umbrella sampling.

☆ This article is part of a Special Issue entitled: Biosimulations edited by Ilpo Vattulainen and Tomasz Róg.

* Corresponding author at: Molecular Structure and Function, The Hospital for Sick Children, 686 Bay Street, Toronto, Ontario M5G 0A4, Canada
E-mail address: pomes@sickkids.com (R. Pomès).

http://dx.doi.org/10.1016/j.bbamem.2016.03.006
0005-2736/

was provided by Lyman and Patel [31]; and reviews of molecular transport across lipid bilayers and the importance of membrane defects were provided by Loverde [32] and Bennett and Tieleman [33].

2. Bilayer PMFs from recent free energy simulations

In the past three years, bilayer PMFs for more than 100 small molecules have been reported in at least forty publications [34–75]. All of these studies utilized bilayers with homogeneous phospholipids (Table S1), with three studies also including varying concentrations of cholesterol [41,50,53]. Furthermore, these free energy simulations involved only three types of phospholipid headgroup. The overwhelming favorite (93% of publications) is the zwitterionic phosphatidylcholine (PC) headgroup, although anionic phosphatidylserine (PS) [37] and phosphatidylglycerol (PG) [60,71] were also considered (Table S1 and Fig. 1A). The distribution of acyl chain lengths and their degree of unsaturation, and hence the bilayer thickness and elasticity [76], in these simulations was substantially broader. Nevertheless, there is a preponderant use of palmitoyl, oleoyl, and myristoyl chains, which together comprised 93% of the acyl chain combinations used in these simulations (Table S1 and Fig. 1A). This reliance on homogenous bilayers composed of a few combinations of lipid headgroups and acyl chains presents the advantage of avoiding sources of sampling error associated with more complex membrane mimetics, including lipid mixtures. We note that similar simplifications are also employed in some experimental studies of solute-membrane interactions [77–81].

The first and most popular scheme to describe computed bilayer PMFs and their underlying intermolecular interactions conceptually divides the bilayer into four regions based on the displacement from its center of mass, $|z|$ [82,83]. We and others have recently proposed alternative schemes with minor distinctions in the chemical composition of the different regions [84,85]. Here, we introduce a new shape-based scheme to classify bilayer PMFs (outlined in Fig. 1C–F), which we view as complementary to the existing four-region models. This scheme is based on the free energy along $|z|$, $\Delta G(|z|)$, when moving from water to the bilayer center. Succinctly, type-1 PMFs increase monotonically, type-2 PMFs decrease monotonically, and type-3 PMFs first decrease and then increase. The letter "b" is added to indicate an initial free energy barrier along $|z|$, which is often but not necessarily due to solute interactions with lipid headgroups. Finally, a star indicates that the value of $\Delta G(|z|)$ at the bilayer center is greater than or equal to its value in bulk water. To avoid overcomplicating this scheme, type-3 PMFs also include cases with a shallow secondary minimum at $z = 0$.

The bilayer PMFs published in the last three years are categorized with the aforementioned shape-based scheme in Table S1 and Fig. 1B. This analysis leads to the following three conclusions. First, most bilayer PMFs (91%) have a free energy barrier along $|z|$ near the bilayer center, which is only lacking in types 2 (6%) and 2b (3%) (Fig. 1B). Second, most bilayer PMFs (84%) do not have an initial free energy barrier along $|z|$, which is only present in types 2b (3%), 3b (6%), and 3b* (7%) (Fig. 1B). Finally, the most common shape of a bilayer PMF (63%) has values of $\Delta G(|z|)$ that first decrease and then increase toward the bilayer center, where the central barrier along $|z|$ is either relatively small (type 3, 25%) or large (type 3*, 38%) (Fig. 1B). Note that this analysis reflects the specific solute/lipid combinations used in recent computations and that these conclusions do not necessarily apply to the entire set of solutes that may interact with lipid bilayers or cell membranes.

Representative examples of each of the shape-based bilayer PMF classifications are provided in Table 1 and all the bilayer PMFs published in the past three years and considered in this review are listed in Table S1. Out of these 201 PMF profiles, only that of Paracetamol in DPPC does not fit the proposed scheme, having a global minimum at the bilayer surface, a high barrier to bilayer entry, and a local minimum at the bilayer core, which, at 20 kcal/mol, is much more substantial than the shallow central local minimum present in some of the other PMFs [73].

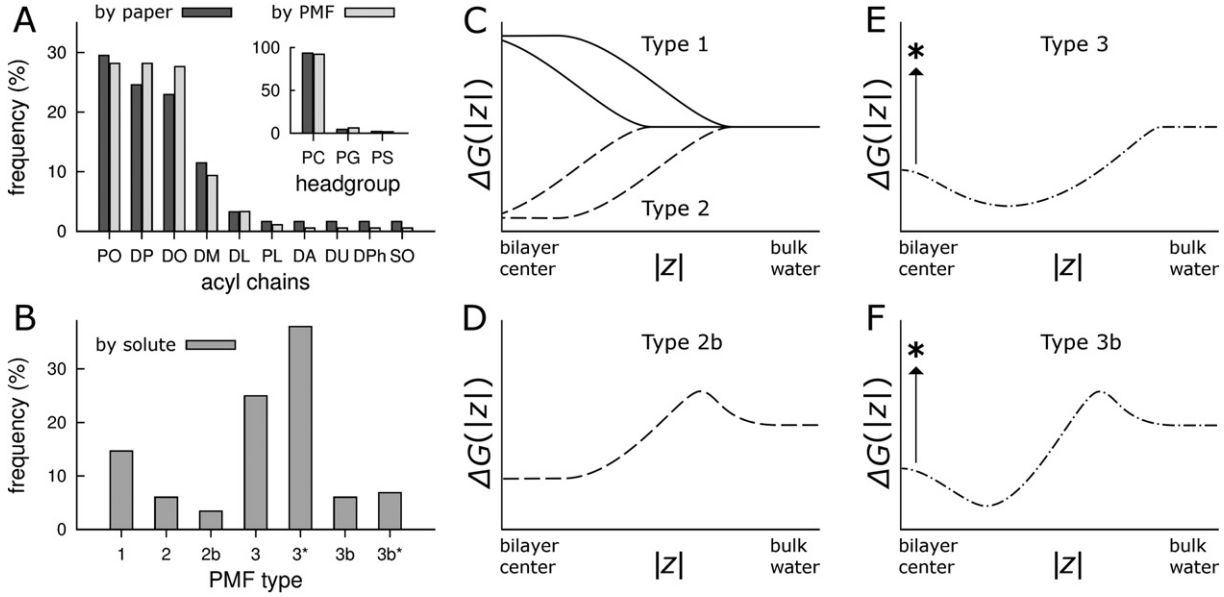

Fig. 1. Lipids used in recent free energy simulations and classification of bilayer PMFs. (A) Relative frequency of different types of lipid acyl chains and (inset) headgroups calculated (dark gray) by publication and (light gray) by PMF. Acyl chain identifiers are: (PO) palmitoyl-oleoyl, (DP) dipalmitoyl, (DO) dioleoyl, (DM) dimyristoyl, (DL) dilauroyl, (PL) palmitoyl-lauroyl, (DA) diarachidonoyl, (DU) dilinoleoyl, (DPh) diphytanoyl, and (SO) stearoyl-oleoyl. Headgroup identifiers are: (PC) phosphatidylcholine, (PG) phosphatidylglycerol, and (PS) phosphatidylserine. (B) Relative frequencies of different types of bilayer PMFs. (C–F) Schematic representation of the different shapes of bilayer PMFs vs. the distance between the centers of mass of the solute and the bilayer along the bilayer normal, $|z|$. (C) Profiles in which the PMF, $\Delta G(|z|)$, increases or decreases monotonically upon insertion are classified as (solid lines) type 1 and (broken lines) type 2, respectively; there may also be a plateau region. (D) Type 2b is similar to type 2 except that the "b" indicates the presence of an initial free energy barrier. (E) Type 3 has favorable binding followed by a free energy barrier near the bilayer center. (F) Type 3b is similar to type 3 except that the "b" indicates the presence of an initial free energy barrier. The star superscript in types 3* and 3b* indicates that the value of $\Delta G(|z|)$ near the bilayer center is larger than in bulk water. PMFs profiles of type 1, 3, 3*, 3b, and 3b* may also feature a shallow secondary well at the bilayer center.

Table 1
Representative solutes for each of the shape-based bilayer PMF types (see Fig. 1).

PMF shape	Solute	Lipid	Ref.
1	Water	POPC, DPPC, DLPS	[34–38]
2	1,3,5-trichlorobenzene	POPC	[48]
2b	Molecular oxygen	DPPC, POPC	[39,44]
3	Hydrogen peroxide	POPC	[39]
3*	Glycine	DPPC	[62,63]
3b	Lidocaine	DMPC	[48]
3b*	Propanol	DMPC	[54,55]

3. Sources of systematic sampling error

Systematic sampling errors arise when large free energy barriers in orthogonal degrees of freedom, also referred to as hidden free energy barriers, trap the sampling in metastable states [86,87]. These errors can be minimized by ensuring that the order parameter(s) used to bias sampling in free energy simulations contain all of the free energy barriers that both separate states of interest and are substantially larger than the available thermal energy. Unfortunately, the shape of the free energy surface and the magnitude of the relevant free energy barriers are generally unknown at the outset of a free energy simulation, whose primary aim is often to characterize these very features. However, a number of studies have identified sources of systematic sampling errors in free energy simulations of solute-bilayer interactions, which are surveyed in this section.

3.1. Arginine side chain and other PMFs of types 1 and 3

The arginine side-chain analog *n*-propylguanidinium has a type-3* PMF in zwitterionic DOPC, POPC, and DPPC bilayers [65,66,84,88,89], although the PMF profiles of both *n*-propylguanidinium and the lysine side-chain analog butylammonium are quantitatively sensitive to force field parameters [65]. As *n*-propylguanidinium approaches a bilayer from aqueous solution, favorable charge–charge interactions are maximized as the cationic guanidino group orients to face the bilayer and nearby lipids stretch toward it [84]. Its orientation is reversed as $|z|$ decreases toward the global free energy minimum and the solute becomes embedded as a mini-detergent in the bilayer, which invaginates slightly around it [84]. A large input of free energy is henceforth required to draw this cation toward the bilayer center as it remains solvated by water and lipid headgroups, which induces a large defect in the bilayer's proximal leaflet [65,66,84,88,90]. Similar side-chain orientations are observed when arginine is located at varying insertion depths in a transmembrane helix, though in this case the free energy minimum is abolished, resulting in a type-1 PMF [42,91].

By comparing bilayer PMFs for *n*-propylguanidinium from different studies, it is possible to identify values of $|z|$ at which the mean force changes systematically with increasing sampling. These locations correspond to: (a) initial bilayer-solute contact, (b) passage of the solute across the headgroup region, where a flip in solute orientation is coupled to a switch in the local deformation of the bilayer from a protrusion to an invagination, and (c) across the bilayer center, where the solute orientation and the identity of the leaflet hosting the solvating defect both invert, possibly involving the formation of a water pore [66]. This analysis strongly suggests that these three locations along $|z|$ are sites of hidden free energy barriers arising from the coupling of solute orientation and local bilayer deformation (Fig. 2). Similar patterns of bilayer distortion are observed for other cationic solutes such as butylammonium [65], methylammonium [42], protonated tyramine [44], and monatomic ions [40], in addition to acetate [90] and neutral molecules with polar moieties such as lipids [92–94], long amphiphiles [61], and alprenolol [85]. The bilayer PMF of a blocked tryptophan residue (type 3) also contains a hidden free energy barrier at the bilayer center related to solute reorientation [95] and solvation [96], as does oleic acid, though the insertion of this latter solute does not result in bilayer invagination at $|z| = 0$ [97].

The invagination of the bilayer upon solute penetration implies that the free energy cost of desolvating ionic solutes exceeds the cost of bilayer deformation and hence that the magnitude of the central free energy barrier depends to a large extent on the bilayer's thickness and bending modulus. Indeed, the magnitude of this barrier correlates with bilayer thickness in PMFs of lysine and arginine side-chain analogs in their charged states, which induce bilayer defects, whereas their neutral states leave the bilayer core relatively unperturbed [42]. Furthermore, bilayer PMFs of the single-chain phospholipid drug miltefosine indicate that the magnitude of the central free energy barrier decreases with shortening and desaturation of acyl chains in bilayer lipids [50], both of which increase the bilayer's flexibility [76]. Finally, cholesterol, which orders and rigidifies lipid bilayers [98], reduces bilayer invagination in response to solute invasion [93]. This relationship between defect formation and bilayer flexibility explains why the bilayer defects that solvate charged and polar solutes originate from the proximal leaflet; a solvating defect in the distal leaflet would have to be comparatively larger to access the solute and is therefore expected to be more costly.

Once a charged solute crosses the bilayer center, the defect should be most energetically favorable in the other (now proximal) leaflet. However, this is not always the case in US simulations of finite duration [66]. When *n*-propylguanidinium is offset from the bilayer center by a small amount ($0 < |z| \leq 0.2$ nm for POPC), a defect in the distal leaflet is metastable and may persist for more than 1 μs of sampling per umbrella [66]. Despite the fact that 0.2 nm is small in comparison to the bilayer width, this type of systematic sampling error inverts the slope of the PMF in a region where the absolute value of the mean force is quite large and this sampling error can reduce the estimated magnitude of the central barrier by more than 2 kcal/mol [66].

In cases where hidden free energy barriers involve solute reorientation, it is reasonable to presume that sampling errors will be exacerbated by intermolecular interactions that restrict solute mobility. Similar to other solutes with type-3 PMFs, protonated clozapine is orientationally restricted by the necessity for its charge group to snorkel toward the headgroup region of the proximal bilayer leaflet [56]. Interestingly, when clozapine is embedded in the bilayer in US simulations, the addition of a second proton (overall solute charge of $+2$) dramatically slows solute reorientation about the bilayer normal, which Ma et al. attribute to the simultaneous interaction of two separate charged groups with bilayer lipids [56]. While the effects of multiple distinct charge groups on the timescales or methods required to attain equilibrium sampling remain to be quantified, such species should be treated with additional caution because of the potential for slow solute reorientation.

3.2. Leucine side chain as a type-2b PMF

The leucine side-chain analog methylpropane has a type-2b PMF in a zwitterionic DOPC bilayer [84,88]. As this hydrophobic solute approaches a bilayer from aqueous solution in US simulations, there is a free energy barrier along $|z|$ as the nearby lipid headgroups slightly invaginate to avoid the solute [84]. However, this bilayer reorganization occurs spontaneously on the low ns timescale [84], suggesting that it does not introduce a substantial hidden free energy barrier. From here, the free energy decreases toward the bilayer center [84,88] with the bilayer forming a local protrusion to encapsulate the solute in its hydrophobic interior for values of $|z|$ slightly under the mean position of lipid headgroup phosphorus atoms [84] (Fig. 3). The evaluation of the mean forces acting on the solute along $|z|$ from different studies of the same simulation system indicates that this encapsulation of methylpropane is generally rapid but can take more than 25 ns per umbrella for values of $|z|$ within 0.1 nm of the transition point in lipid organization and that the time required for this reorganization depends on the initial conformation of the system [84]. As we noted above for

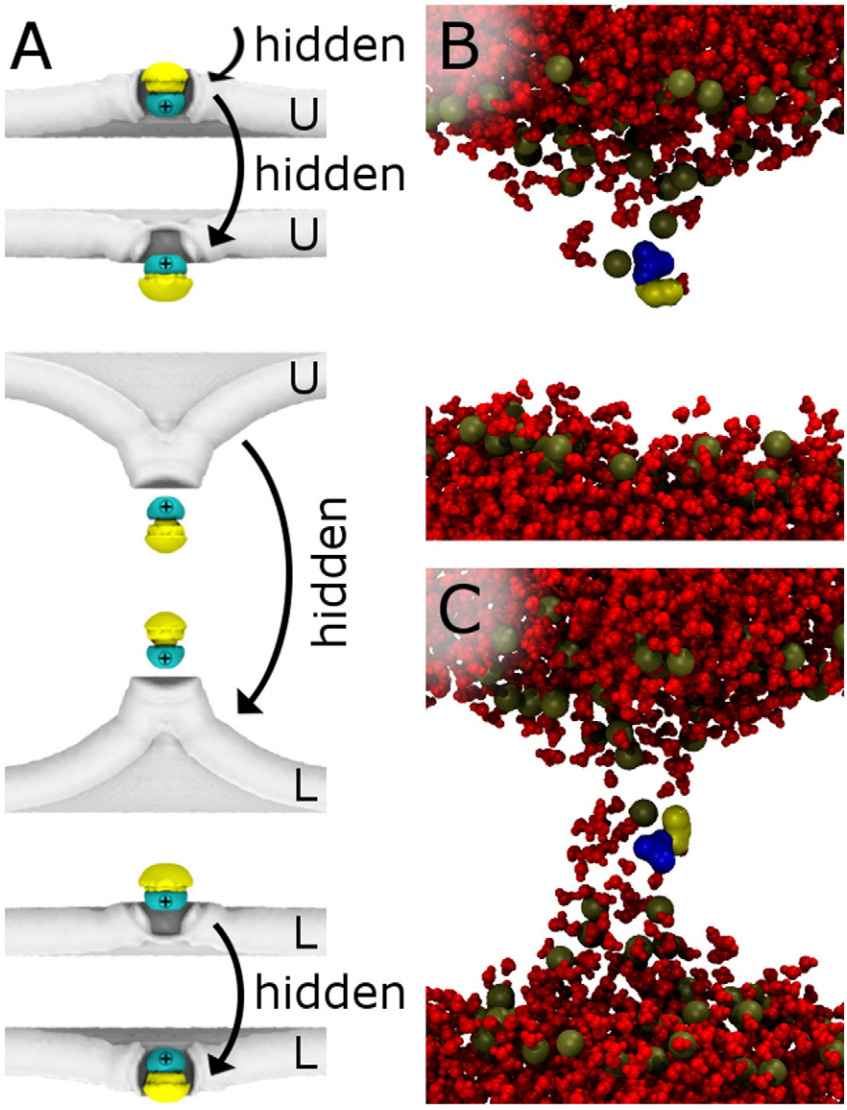

Fig. 2. Bilayer distortion and hidden free energy barriers underlying systematic sampling errors in free energy simulations of the arginine side-chain analog *n*-propylguanidinium. (A) Spatial distribution functions of *n*-propylguanidinium and the proximal bilayer leaflet viewed from the side, looking along the plane of the bilayer showing (gray) phosphorus atoms behind the solute, and (yellow) hydrophobic and (cyan) hydrophilic moieties of the solute. Vertically from top to bottom, the solute passes from water into the (U) upper bilayer leaflet, then into and finally across the (L) lower leaflet. Locations of hidden free energy barriers are marked with curved arrows. (B and C) Bilayer defect for $|z| \sim 0$ nm when there is (B) a defect in the upper leaflet and (C) a water pore. Lipid headgroup phosphorus atoms are shown as large brown spheres, water is shown as small red spheres, and *n*-propylguanidinium heavy atoms are shown in a surface representation with the acyl chain in yellow (C_β,C_γ,C_δ) and the charged guanidino group in blue (N_ε, C_ζ, $N_{\eta 1}$, $N_{\eta 2}$). Reprinted (adapted) with permission from refs. [66] and [84]. Copyright 2011, 2013 American Chemical Society.

bilayer PMFs of *n*-propylguanidinium, systematic sampling errors leading to inaccurate estimates of the mean force over relatively small ranges of $|z|$ can have a substantial impact on the overall estimate of the binding free energy and partition coefficient computed between two states that themselves do not suffer from systematic sampling errors. In the case of methylpropane, sampling errors present in a 0.1-nm-wide $|z|$ interval lead to a $\Delta G(|z|)$ inaccuracy of 1 kcal/mol or approximately 20% of the binding free energy [84].

3.3. Larger solutes

In general, solutes in lipid bilayers can adopt many possible arrangements differing in solute conformation, solute orientation, solute-lipid interactions, bilayer conformation, and extent of insertion. In the regions of $|z|$ where such degeneracies arise, simulations must not only escape initial conformational states with unfavorable free energies but must subsequently exchange between multiple basins of low free energy many times in order to yield estimates of their relative populations, a precondition to attain converged estimates of equilibrium properties including the mean force along the order parameter. As the solute increases in size and conformational complexity, US simulations may suffer more acutely from systematic sampling errors. Thus, the nature and the extent of interaction between a lipid bilayer and a relatively long and rigid solute such as an alpha-helix or a carbon nanotube depends strongly on the solute's orientation relative to the bilayer normal. The degeneracy of solute-lipid interactions, solute orientation, and solute conformation rises sharply with solutes of increasing flexibility. For example, at certain values of $|z|$ corresponding to the approach of the solute near the lipid bilayer, a disordered peptide may form direct interactions with the bilayer in extended conformations but not in compact ones. In such a case, attaining converged estimates of the bilayer PMF requires many spontaneous transitions of the solute's conformation. This type of systematic sampling error was analyzed in US simulations of the antimicrobial peptide indolicidin (Fig. 4) [99] and has been reported for the substantially smaller solute ubiquinone-2 [46].

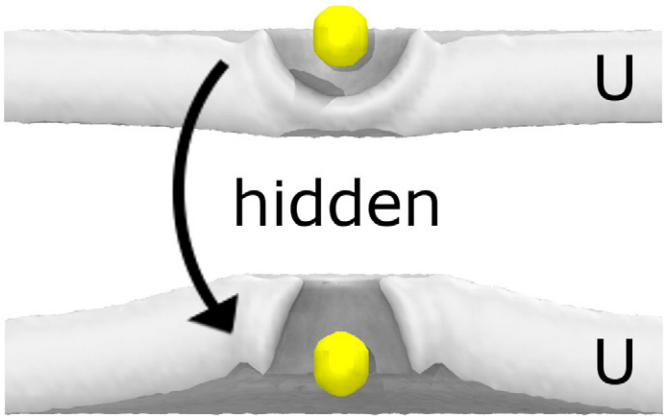

Fig. 3. Bilayer deformation and hidden free energy barrier underlying systematic sampling errors in free energy simulations of the leucine side-chain analog methylpropane. Spatial distribution function of (yellow) methylpropane and (gray) the upper, proximal bilayer leaflet, U, viewed from the side, looking along the plane of the bilayer. Reprinted (adapted) with permission from ref. [84]. Copyright 2011 American Chemical Society.

3.4. Bilayer size

Comer et al. used the adaptive biasing force method [100] to evaluate the influence of the number of lipid molecules on the type-1 bilayer PMF of water [38]. In this study, the authors used a definition of $|z|$ based on the distance between the center of mass of a tagged water molecule and that of the lipid phosphorus and nitrogen atoms and found that the magnitude of the free energy barrier to water permeation did not depend on bilayer size between 20 and 50 lipids per leaflet, although the central free energy barrier became narrower when the number of lipids was increased [38]. Comer et al. attributed this narrowing of the central free energy barrier to the greater ease with which the larger bilayer could undergo local distortions to accommodate the inserted water molecule and facilitate its partial hydration [38]. The influence of membrane undulations on the definition of the membrane normal has also been investigated by Braun et al. [101].

Hu et al. used a similar approach to compute the bilayer PMF of methylguanidinium across a DMPC bilayer with either 32 or 144 lipid molecules per leaflet and found that increasing the bilayer size by a factor of 4.5 permitted a larger bilayer defect and reduced the height of the central free energy barrier along $|z|$ by a factor of two [64]. The authors also noted that the distal leaflet was more perturbed in the smaller bilayer than in the larger bilayer and hypothesized that the size of the bilayer may affect its relative tendency to form single-leaflet defects or water pores [64], similar to the findings of Huang and García [102] (see Section 6.1). However, larger bilayers permit larger undulations, which Kopelevich has shown to be the source of artifacts in which the PMF can appear to tunnel through free energy barriers along $|z|$ [103]. For example, consider the type 2b PMF of methylpropane, which contains a free energy barrier due to unfavorable insertion of this hydrophobic solute in the headgroup region of the bilayer [84]. As the size of the bilayer increases, so does the magnitude of the undulations that it can support. For a given $|z|$ position, a larger bilayer patch permits fluctuations of large enough amplitude to sample both fully-hydrated and fully-inserted states of the solute. If the bilayer is sufficiently large, there may be no z-restrained positions that predominantly sample the real barrier to solute insertion, leaving only a barrier based on loss of system entropy that is expected to vanish as the simulation system increases in size. Using a nanoparticle solute and a DPPC bilayer with approximately 300 lipids per leaflet, Kopelevich goes on to show that some of the states of extensive bilayer protrusion (with concurrent encapsulation of the hydrophobic solute) that are highly populated in US simulations with a flexible bilayer are not representative of unrestrained binding events [103], a conclusion that we have also reached for methylpropane in DOPC bilayers with only 32 lipids per leaflet [84]. Kopelevich's resolution of this sampling dilemma is to fix the headgroups of the lipids in the distal leaflet, which appears to be an excellent solution except in cases where the distal leaflet is expected to undergo distortions in response to solute binding.

We conclude this section on the relevance of bilayer size with an illustrative conjecture. Given a sufficiently large bilayer and defining $|z|$ as the distance between the centers of mass of the solute and the bilayer, a solute at $|z| = 0$ may not form any direct contact with the bilayer, thereby sampling an irrelevant region of phase space and yielding a PMF with no real predictive value (Fig. 5).

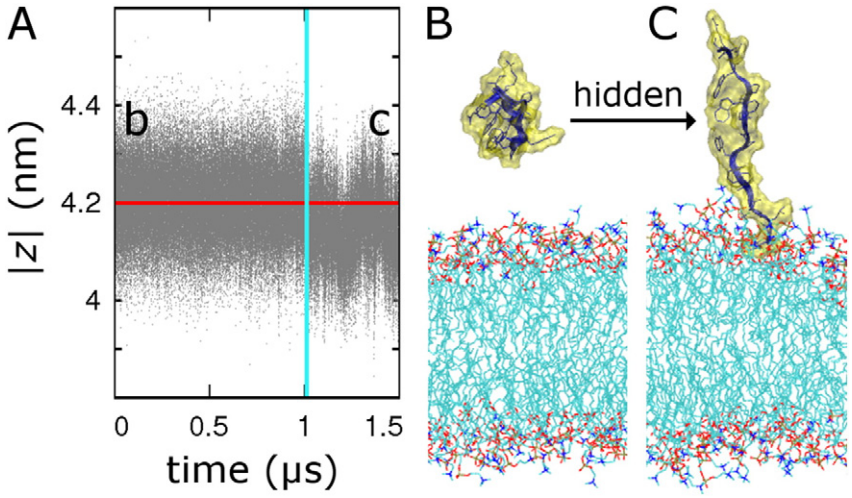

Fig. 4. Slow relaxation across a hidden free energy barrier for a relatively large solute near a lipid bilayer. (A) Time-series of the distance between the centers of mass of a POPC bilayer and of the 14-residue antimicrobial peptide indolicidin, $|z|$, with an umbrella sampling bias centered at 4.2 nm (red horizontal line). After 1 μs of sampling, the peptide extends and makes favorable ionic contacts with the headgroups of bilayer lipids, affecting both the mean and the variance of $|z|$, which directly impact the PMF [99]. (B and C) Representative conformations of the simulation system (B) before and (C) after the conformational transition.

Fig. 5. Given sufficiently large bilayer undulations, the centers of mass of a solute and the lipid bilayer can coincide without direct physical contact.

3.5. Initial conformation

Paloncýová et al. computed the type-3 bilayer PMF of coumarin in DOPC and DOPG [60,104] and evaluated the influence of starting conformation and the method used to maintain the solute at different bilayer immersion depths [104]. The z-constraint method [82] and US generated statistically indistinguishable bilayer PMFs of coumarin in DOPC when initial conformations were drawn from unrestrained simulation [104]. However, the PMFs from these biased simulations varied systematically with the method used to generate initial conformations. Specifically, initial conformations generated from nonequilibrium pulling simulations retained systematic sampling errors throughout 50 ns of sampling per umbrella or window, leading to a binding free energy inaccuracy of ~1 kcal/mol or about 15% [104].

Intriguingly, in a study of long amphiphiles (7-nitrobenz-2-oxa-1,3-diazol-4-yl-labeled fatty amines) interacting with lipid bilayers, Filipe et al. showed that restrained simulations are less susceptible to long-lived systematic sampling errors when initial conformations are constructed by pulling the solute away from the bilayer center out into bulk water rather than in the opposite direction, from water toward the bilayer center [61]. These long amphiphiles must flip about the bilayer plane as they pass through the water-lipid interface in equilibrium simulations [61], similar to the $|z|$-dependent orientational preferences of the short amphiphile *n*-propylguanidinium (Fig. 2) [84]. This difference in relaxation timescales based on the pulling direction could indicate that the hidden free energy barrier is smaller closer to the bilayer center. US simulations of the antimicrobial peptide indolicidin, which can adopt amphiphilic structures, also suggest that generating initial conformations by pulling the solute into the bilayer from water biases the PMF toward the unbound state on the 25 ns/umbrella timescale [99,105]. In this case, systematic sampling errors were reduced when initial conformations were generated by separately embedding the peptide at each $|z|$ position, although US simulations still required ≥4 μs/umbrella to attain converged estimates of the PMF [99]. While it remains to be seen whether systematic sampling errors involving solute orientation depend on the vector used in an initial non-equilibrium pulling procedure for a variety of solute-bilayer combinations, evaluating PMFs from two separate sets of simulations prepared by pulling in opposite directions (or, alternatively, by pulling across the entire bilayer in a single direction) should reveal any hysteresis resulting from slow relaxation, paralleling the backward and forward approach adopted by Pearlman and Kollman in slow growth free energy perturbation simulations [106]. This approach should be an excellent way to identify the existence of systematic sampling errors and the regions of $|z|$ that host hidden free energy barriers.

Finally, the initial conformation of the lipid bilayer, coupled with the initial conformation and location of a solute, can influence whether the composite system adopts a metastable conformation with a locally favorable but globally unfavorable free energy. For instance, our current research suggests that for *n*-propylguanidinium near $|z| = 0$ in a POPC bilayer, the leaflet(s) in which the solvating defect initially forms depends more strongly on the initial conformation of the bilayer than on the initial orientation of the solute (unpublished data). Thus, random fluctuations in bilayer thickness may induce the formation of a persistent metastable defect in the distal leaflet (see Section 3.1). This finding highlights the importance of varying bilayer conformation in addition to solute conformation and orientation when assessing systematic sampling errors, a factor that is expected to become increasingly relevant with increasing lipid heterogeneity.

4. Force-field dependence of bilayer defects

As outlined in Section 3.1, the mean force acting on a charged solute embedded near the bilayer center is largely determined by the presence of a defect that brings water and lipid headgroups of one or both leaflets into the bilayer's hydrophobic core. Therefore, the extent to which a bilayer PMF is affected by sampling errors depends on the free energy of defect formation for a given force field. Unexpectedly, the likelihood of forming such defects, which is intricately tied to the bilayer's bending modulus, can depend with exquisite sensitivity on the truncation of Lennard-Jones interactions. Specifically, Huang and García showed that when the phosphorus atom of a constituent lipid molecule is brought to the center of a DPPC bilayer using the Berger lipid parameters [107], the bilayer reproducibly forms a double defect (i.e., a pore) when the Lennard-Jones cutoff radius $r_c = 0.9$ nm and forms a defect involving invagination of only one leaflet when $r_c \geq 1.0$ nm, presumably because as r_c decreases the bilayer becomes thinner, thus facilitating water penetration [108]. This change in solvation dramatically affects the resulting bilayer PMF [108]. Conversely, the PMF of water insertion into a POPC bilayer, which also results in bilayer deformation, is largely unaffected by reducing r_c from 1.2 to 0.8 nm [38] in simulations employing the CHARMM36 lipid force field [109], likely because the hydrating bilayer defect does not follow the restrained water molecule all the way to the center of a CHARMM36 POPC bilayer [34,38].

The formation of bilayer defects upon solute insertion also depends on the resolution of the molecular model. Specifically, Sun et al. showed that when *n*-propylguanidinium or butylammonium are held at the bilayer center, bilayer defects are largest in all-atom models, intermediate in united-atom models, and smallest (and in some cases nonexistent) in coarse-grained models [65].

5. Detecting hidden barriers

One approach to identifying hidden free energy barriers is simply to evaluate a variety of orthogonal degrees of freedom, searching for those with a sharp or oscillatory dependence on $|z|$. This is not to suggest that a given hidden free energy barrier can only exist on a narrow range of $|z|$, but rather that a sharp transition along an orthogonal variable warrants further investigation.

Recently, a few methods have been introduced that accidentally report on the locations of hidden free energy barriers along $|z|$. All of these methods, which include metadynamics [25], the orthogonal-space random walk [87], and US with replica exchange of umbrellas [110,111], apply biases to impose homogeneous sampling along a prescribed order parameter(s) while simultaneously permitting free movement along that order parameter. Because these procedures amount to "flattening" the free energy surface along the order parameter, regions in which mobility along that order parameter is poor are likely to contain free energy barriers in orthogonal degrees of freedom. To quantify this behavior, we developed a metric called the transmission factor that can be computed from US simulations with replica exchange of umbrellas and used it to a priori identify hidden free energy barriers as *n*-propylguanidinium crosses both the water-bilayer interface and the center of a lipid bilayer [66]. Similarly, the orthogonal-space tempering method was shown to reveal hidden free energy barriers as a solute molecule, H_2S, moved between regions of different bilayer composition [34]. However, the magnitude of the resulting systematic sampling errors in the latter approach is unclear as differences in lipid, force field, and sampling method complicate detailed comparison to another bilayer PMF of H_2S with a significantly different shape [35]. We are unaware of any studies that have used

metadynamics to identify hidden free energy barriers a priori, but the potential for this application is clear because, in the absence of hidden barriers, metadynamics simulations should lead to a true random walk along the order parameter(s) [112–114].

6. Overcoming hidden barriers

Two main strategies can be used to alleviate systematic sampling errors. First, one can identify and rationally circumvent the free energy barriers that impede sampling by using either better initial conformations, as discussed in Section 3.5, or better order parameter(s), as discussed below (Section 6.1) The second approach is simply to perform more sampling, which can be achieved by incorporating multiple solute molecules into a single simulation system (Section 6.2).

6.1. Order parameter modifications

By far the most commonly used order parameter in free energy simulations of solute-bilayer interactions is the distance between the center of mass of the solute and that of the bilayer along the bilayer normal. In principle, the order parameter in a PMF calculation should include the slowest transitions of relevance, so that all other degrees of freedom are correctly averaged out. The existence of persistent systematic sampling errors, as reviewed above, demonstrates that this commonly-used order parameter is inadequate for many, if not most, calculations of bilayer PMFs. However, the selection of the optimal order parameter is a challenging problem. For example, Hinner et al. showed that the convergence properties of the bilayer PMF of the dye di-4-ASPBS are dramatically affected by the region of the solute used to define $|z|$ [115]. Specifically, when the restraint acts on the acidic headgroup of this zwitterion, convergence of the PMF is attained relatively rapidly near the bilayer center, but very slowly at the water-bilayer interface [115]. Conversely, when the restraint acts on the solute's center, the rate of convergence is intermediate at both extremes [115].

To alleviate the influence of severe membrane distortion on the PMF and its rate of convergence, some researchers have chosen instead to modify the region of the bilayer that is used in the definition of the solute's displacement. Specifically, Filipe et al. demonstrated that an order parameter with a cylindrical boundary that dynamically defines a subset of nearby lipids [116] leads free energy simulations to converge more rapidly, presumably by reducing the amplitude of fluctuations in local lipid structure [61]. This cylindrical definition of $|z|$ has also been used by Zocher et al., among others, to reduce the PMF's dependence on membrane undulations [41]. Separately, Huang and García conducted US simulations in which the definition of $|z|$ was based on the position of the C_ζ atom of a single residue of a cyclic arginine nonamer and a dynamic selection of lipids within a very small (0.5 nm) cylindrical radius [102]. Near $|z| = 0$ this formulation led to the formation of a pore that substantially reduced the free energy of peptide translocation compared to the pore-free, single-defect translocation predicted by simulations that defined $|z|$ based on the center of mass of all lipids [102]. Essentially, this cationic peptide recruited lipids from one leaflet toward the bilayer center and the small radius of the cylindrical cutoff enforced the simultaneous approach of lipids from the other leaflet. The use of a cylindrical boundary potential in the dynamic selection of lipids that define $|z|$ may also protect against artifacts due to bilayer asymmetry resulting from spontaneous lipid flip flop, a process whose rate can be dramatically enhanced by using lipids with short acyl chains [92] or via the presence of charged or polar solutes near the bilayer center [66].

In a slightly different approach, Mao et al. evaluated the binding of monatomic cations to POPC and POPG bilayers using an order parameter based on the distance between the solute and its nearest lipid phosphorus atom [117]. It is unclear if this approach is applicable to larger solutes and PMFs across the entire lipid bilayer.

Lin and Grossfield recently introduced a radically different order parameter based on the extent of solute-lipid interactions and eschewing distance restraints altogether [118]. The insertion of an antimicrobial lipopeptide micelle into a lipid bilayer was enforced in US simulations by dialing up the number of hydrophobic contacts between the lipopeptide molecules of the solute and the lipid molecules of the bilayer. This approach allowed the authors to capture the rate-limiting steps in the insertion process. The sampling efficiency of this study, especially considering the size and the complexity of the solute, is due in part to the use of a coarse-grained potential, which smoothens the energy landscape. In addition, its focus on solute–solvent interactions is well suited to the dissolution of a molecular aggregate into the bilayer, which cannot be captured with insertion depth alone.

Accordingly, another strategy to reduce systematic sampling errors in bilayer PMFs computed along $|z|$ is to increase the dimensionality of the order parameter. In an atomistic study using a bias-exchange metadynamics framework and the approach of Ghaemi et al. [119], Galassi and Arantes showed that the number of contacts between the solute and lipid or water molecules is an important degree of freedom orthogonal to $|z|$ that can be used to enhance sampling for amphiphilic ubiquinones with long hydrophobic chains [46]. Given that lipid headgroups are involved in the vast majority of the hidden free energy barriers covered in this review, this approach appears well suited to the task at hand.

For solutes with complex intramolecular landscapes, it may also be useful to use multidimensional order parameters that control solute conformation, an approach taken by Jämbeck and Lyubartsev to sample the substantial free energy barriers controlling the conformational isomerization of Aspirin and Ibuprofen [59].

6.2. Simulations with multiple solute molecules

The slow convergence of bilayer PMFs underscores the need for strategies to improve the efficiency of simulations. For small solutes, such an improvement may be achieved trivially, by placing multiple solute molecules in the same simulation box. Bemporad et al. computed the bilayer PMFs of water and other small molecules using simulation systems containing five solute molecules restrained to different values of $|z|$ [120], thus obtaining five times more sampling per unit of computational resource than would have been achieved with a single solute in the simulation cell. Similarly, MacCallum et al. computed the bilayer PMFs of amino acid side-chain analogs using two solute molecules per simulation cell, thus doubling computational efficiency without affecting the resulting PMF of *n*-propylguanidinium [88]. This approach has also been used by Arcario et al. to study anesthetics [72] and has been extended to include solute separation in the bilayer plane, in some cases using up to 20 solutes per simulation without changing the bilayer PMF of tryethylamine [41]. However, given the large bilayer distortions induced by some solutes [40,42,44,61,65,66,84,85,88,90,92–94,96,97] and the cooperative binding of solutes such as *n*-propylguanidinium [121], it is possible that unexpected cooperative or anti-cooperative effects exist for certain solutes even when they are far apart from one another. Therefore, this approach deserves special caution.

7. Conclusions

Using molecular simulations to quantify the interaction of molecular solutes with lipid bilayers is an active area of research. Although free energy simulations of solute-bilayer systems have become routine, it has recently become apparent that even simulations of simple solutes are prone to significant systematic sampling errors. In this review, we have presented recent progress in computing free energy profiles for inserting molecular solutes into lipid bilayers together with a detailed analysis of the sources and the nature of systematic sampling errors affecting these simulations. Such errors are due to slow relaxation in degrees of freedom orthogonal to the order parameter(s). When the order parameter is the commonly-used insertion depth of the solute, such "hidden barriers" frequently occur during solute adsorption, insertion,

and translocation across the bilayer center. These hidden barriers depend on the interactions of the solute with water molecules, lipid headgroups, and lipid acyl chains, and reflect the visco-elastic nature of the bilayer.

The sources of these systematic sampling errors can be generally formulated in terms of degeneracy of the free energy landscape along the order parameter or reaction coordinate—degeneracy of the solute conformations and orientation as well as of solute-bilayer interactions and bilayer deformations. To tackle this degeneracy, different approaches may be used. The simplest, most general recommendation consists of using multiple replicas starting from different bilayer conformations as well as different solute conformations and orientations, which may include different initial states obtained by moving the solute in opposite directions along the membrane normal. In addition, using replica exchange (or other methods involving a random walk of the solute along the membrane normal) not only reveals the loci of systematic sampling errors but also helps bypass insertion-depth-dependent barriers impeding solute reorientation, conformational isomerization, and reorganization of the bilayer.

Arguably the most promising strategy to improve the efficiency and the accuracy of free energy simulations of solute binding to lipid bilayers is to use novel order parameters that accelerate the crossing of these hidden barriers. Of particular interest is the approach taken in two recent studies, in which the order parameter either consisted of [118] or included [46] a count of solute-lipid contacts. The long-term success of contact-based order parameters may depend on whether or not they are applicable to a broad range of molecular solutes and lipid bilayers.

Transparency document

The transparency document associated with this article can be found, in online version.

Acknowledgments

We gratefully acknowledge support from the Canadian Institutes of Health Research (CIHR) for a Fellowship to CN and from the Natural Sciences and Engineering Research Council (NSERC) for Discovery Grant RGPIN 418679 to RP.

Appendix A. Supplementary data

Supplementary data to this article can be found online at http://dx.doi.org/10.1016/j.bbamem.2016.03.006.

References

[1] G. Quincke, Ueber periodische ausbreitung an flüssigkeitsoberflächen und dadurch hervorgerufene bewegungserscheinungen, Ann. Phys. 271 (1888) 580–642.
[2] S.J. Singer, G.L. Nicolson, The fluid mosaic model of the structure of cell membranes, Science 175 (1972) 720–731.
[3] E. Gorter, F. Grendel, On biomolecular layers of lipoids on the chromocytes of the blood, J. Exp. Med. 41 (1925) 439–443.
[4] J.N. Israelachvili, D.J. Mitchell, B.W. Ninham, Theory of self-assembly of hydrocarbon amphiphiles into micelles and bilayers, J. Chem. Soc. Faraday Trans. 72 (1976) 1525–1568.
[5] J.D. Robertson, The ultrastructure of cell membranes and their derivatives, Biochem. Soc. Symp. 16 (1959) 3–43.
[6] H. Nikaido, Molecular basis of bacterial outer membrane permeability revisited, Microbiol. Mol. Biol. Rev. 67 (2003) 593–656.
[7] D.M. Prescott, E. Zeuthen, Comparison of water diffusion and water filtration across cell surfaces, Acta Physiol. Scand. 28 (1953) 77–94.
[8] S. Paula, A.G. Volkov, A.N. Van Hoek, T.H. Haines, D.W. Deamer, Permeation of protons, potassium ions, and small polar molecules through phospholipid bilayers as a function of membrane thickness, Biophys. J. 70 (1996) 339–348.
[9] J.C. Skou, Enzymatic basis for active transport of Na + and K+ across cell membrane, Physiol. Rev. 45 (1965) 596–618.
[10] R.M. Hochmuth, C.A. Evans, H.C. Wiles, J.T. McCown, Mechanical measurement of red cell membrane thickness, Science 220 (1983) 101–102.
[11] K. Mitra, I. Ubarretxena-Belandia, T. Taguchi, G. Warren, D.M. Engelman, Modulation of the bilayer thickness of exocytic pathway membranes by membrane proteins rather than cholesterol, Proc. Natl. Acad. Sci. U. S. A. 101 (2004) 4083–4088.
[12] W.C. Wimley, Toward genomic identification of β-barrel membrane proteins: composition and architecture of known structures, Protein Sci. 11 (2002) 301–312.
[13] D.L. Heefner, G.W. Claus, Change in quantity of lipids and cell size during intracytoplasmic membrane formation in Gluconobacter oxydans, J. Bacteriol. 125 (1976) 1163–1171.
[14] J.B. Rattray, A. Schibeci, D.K. Kidby, Lipids of yeasts, Bacteriol. Rev. 39 (1975) 197–231.
[15] G.M. Gray, H.J. Yardley, Lipid compositions of cells isolated from pig, human, and rat epidermis, J. Lipid Res. 16 (1975) 434–440.
[16] A. Finkelstein, A. Cass, Permeability and electrical properties of thin lipid membranes, J. Gen. Physiol. 52 (1968) 145–172.
[17] C.V. Paganelli, A.K. Solomon, The rate of exchange of tritiated water across the human red cell membrane, J. Gen. Physiol. 41 (1957) 259–277.
[18] M. Zasloff, Antimicrobial peptides of multicellular organisms, Nature 415 (2002) 389–395.
[19] P. Seeman, The membrane actions of anesthetics and tranquilizers, Pharmacol. Rev. 24 (1972) 583–655.
[20] M. Ansari, M. Kazemipour, M. Aklamli, The study of drug permeation through natural membranes, Int. J. Pharm. 327 (2006) 6–11.
[21] M. Kansy, F. Senner, K. Gubernator, Physicochemical high throughput screening: parallel artificial membrane permeation assay in the description of passive absorption processes, J. Med. Chem. 41 (1998) 1007–1010.
[22] R. Giulia, M. Luca, Modeling the effect of nano-sized polymer particles on the properties of lipid membranes, J. Phys. Condens. Matter 26 (2014) 503101.
[23] G.M. Torrie, J.P. Valleau, Nonphysical sampling distributions in Monte Carlo free-energy estimation: umbrella sampling, J. Comput. Phys. 23 (1977) 187–199.
[24] B. Roux, The calculation of the potential of mean force using computer simulations, Comput. Phys. Commun. 91 (1995) 275–282.
[25] A. Laio, M. Parrinello, Escaping free-energy minima, Proc. Natl. Acad. Sci. U. S. A. 99 (2002) 12562–12566.
[26] Z.E. Hughes, C.J. Malajczuk, R.L. Mancera, The effects of cryosolvents on DOPC–β-sitosterol bilayers determined from molecular dynamics simulations, J. Phys. Chem. B 117 (2013) 3362–3375.
[27] K.E. Norman, H. Nymeyer, Indole localization in lipid membranes revealed by molecular simulation, Biophys. J. 91 (2006) 2046–2054.
[28] C. Chipot, Frontiers in free-energy calculations of biological systems, Wiley Interdiscip. Rev. Comput. Mol. Sci. 4 (2014) 71–89.
[29] J.C. Gumbart, B. Roux, C. Chipot, Standard binding free energies from computer simulations: what is the best strategy? J. Chem. Theory Comput. 9 (2013) 794–802.
[30] N. Hansen, W.F. van Gunsteren, Practical aspects of free-energy calculations: a review, J. Chem. Theory Comput. 10 (2014) 2632–2647.
[31] L. Edward, P. Sandeep, Molecular dynamics of lipid bilayers, in: G. Pabst, N. Kučerka, M.-P. Nieh, J. Katsaras (Eds.), Liposomes, Lipid Bilayers and Model Membranes, CRC Press 2014, pp. 69–98.
[32] S.M. Loverde, Molecular simulation of the transport of drugs across model membranes, J. Phys. Chem. Lett. 5 (2014) 1659–1665.
[33] W.F.D. Bennett, D.P. Tieleman, The importance of membrane defects—lessons from simulations, Acc. Chem. Res. 47 (2014) 2244–2251.
[34] C. Lv, E.W. Aitchison, D. Wu, L. Zheng, X. Cheng, W. Yang, Comparative exploration of hydrogen sulfide and water transmembrane free energy surfaces via orthogonal space tempering free energy sampling, J. Comput. Chem. 37 (2016) 567–574.
[35] S. Riahi, C.N. Rowley, Why can hydrogen sulfide permeate cell membranes? J. Am. Chem. Soc. 136 (2014) 15111–15113.
[36] M. Nategholeslam, C.G. Gray, B. Tomberli, Implementation of the forward–reverse method for calculating the potential of mean force using a dynamic restraining protocol, J. Phys. Chem. B 118 (2014) 14203–14214.
[37] B. Qiao, M. Olvera de la Cruz, Driving force for water permeation across lipid membranes, J. Phys. Chem. Lett. 4 (2013) 3233–3237.
[38] J. Comer, K. Schulten, C. Chipot, Calculation of lipid-bilayer permeabilities using an average force, J. Chem. Theory Comput. 10 (2014) 554–564.
[39] R.M. Cordeiro, Reactive oxygen species at phospholipid bilayers: distribution, mobility and permeation, Biochim. Biophys. Acta Biomembr. 1838 (2014) 438–444.
[40] I. Vorobyov, T.E. Olson, J.H. Kim, R.E. Koeppe II, O.S. Andersen, T.W. Allen, Ion-induced defect permeation of lipid membranes, Biophys. J. 106 (2014) 586–597.
[41] F. Zocher, D. van der Spoel, P. Pohl, Jochen S. Hub, Local partition coefficients govern solute permeability of cholesterol-containing membranes, Biophys. J. 105 (2013) 2760–2770.
[42] L. Li, I. Vorobyov, T.W. Allen, The different interactions of lysine and arginine side chains with lipid membranes, J. Phys. Chem. B 117 (2013) 11906–11920.
[43] Y. Wang, D. Hu, D. Wei, Transmembrane permeation mechanism of charged methyl guanidine, J. Chem. Theory Comput. 10 (2014) 1717–1726.
[44] B.W. Holland, M.D. Berry, C.G. Gray, B. Tomberli, A permeability study of O2 and the trace amine p-tyramine through model phosphatidylcholine bilayers, PLoS One 10 (2015) e0122468.
[45] A. Khajeh, H. Modarress, Effect of cholesterol on behavior of 5-fluorouracil (5-FU) in a DMPC lipid bilayer, a molecular dynamics study, Biophys. Chem. 187–188 (2014) 43–50.
[46] V.V. Galassi, G.M. Arantes, Partition, orientation and mobility of ubiquinones in a lipid bilayer, Biochim. Biophys. Acta Bioenerg. 1847 (2015) 1560–1573.
[47] L. Nierzwicki, M. Wieczor, V. Censi, M. Baginski, L. Calucci, S. Samaritani, J. Czub, C. Forte, Interaction of cisplatin and two potential antitumoral platinum(ii) complexes with a model lipid membrane: a combined NMR and MD study, Phys. Chem. Chem. Phys. 17 (2015) 1458–1468.

[48] J.P.M. Jambeck, A.P. Lyubartsev, Implicit inclusion of atomic polarization in modeling of partitioning between water and lipid bilayers, Phys. Chem. Chem. Phys. 15 (2013) 4677–4686.
[49] H. Wang, X. Ren, F. Meng, Molecular dynamics simulation of six β-blocker drugs passing across POPC bilayer, Mol. Simul. 42 (2015) 56–63.
[50] M. Malta de Sá, V. Sresht, C.O. Rangel-Yagui, D. Blankschtein, Understanding miltefosine–membrane interactions using molecular dynamics simulations, Langmuir 31 (2015) 4503–4512.
[51] P. Podloucká, K. Berka, G. Fabre, M. Paloncýová, J.-L. Duroux, M. Otyepka, P. Trouillas, Lipid bilayer membrane affinity rationalizes inhibition of lipid peroxidation by a natural lignan antioxidant, J. Phys. Chem. B 117 (2013) 5043–5049.
[52] S. Genheden, J.W. Essex, A simple and transferable all-atom/coarse-grained hybrid model to study membrane processes, J. Chem. Theory Comput. 11 (2015) 4749–4759.
[53] T. Ingram, S. Storm, L. Kloss, T. Mehling, S. Jakobtorweihen, I. Smirnova, Prediction of micelle/water and liposome/water partition coefficients based on molecular dynamics simulations, COSMO-RS, and COSMOmic, Langmuir 29 (2013) 3527–3537.
[54] T. Bereau, K. Kremer, Automated parametrization of the coarse-grained Martini force field for small organic molecules, J. Chem. Theory Comput. 11 (2015) 2783–2791.
[55] S. Jakobtorweihen, A.C. Zuniga, T. Ingram, T. Gerlach, F.J. Keil, I. Smirnova, Predicting solute partitioning in lipid bilayers: free energies and partition coefficients from molecular dynamics simulations and COSMOmic, J. Chem. Phys. 141 (2014) 045102.
[56] J. Ma, L. Domicevica, J.R. Schnell, P.C. Biggin, Position and orientational preferences of drug-like compounds in lipid membranes: a computational and NMR approach, Phys. Chem. Chem. Phys. 17 (2015) 19766–19776.
[57] G. Först, L. Cwiklik, P. Jurkiewicz, R. Schubert, M. Hof, Interactions of beta-blockers with model lipid membranes: molecular view of the interaction of acebutolol, oxprenolol, and propranolol with phosphatidylcholine vesicles by time-dependent fluorescence shift and molecular dynamics simulations, Eur. J. Pharm. Biopharm. 87 (2014) 559–569.
[58] Timothy S. Carpenter, Daniel A. Kirshner, Edmond Y. Lau, Sergio E. Wong, Jerome P. Nilmeier, Felice C. Lightstone, A method to predict blood–brain barrier permeability of drug-like compounds using molecular dynamics simulations, Biophys. J. 107 (2014) 630–641.
[59] J.P.M. Jämbeck, A.P. Lyubartsev, Exploring the free energy landscape of solutes embedded in lipid bilayers, J. Phys. Chem. Lett. 4 (2013) 1781–1787.
[60] M. Paloncýová, K. Berka, M. Otyepka, Molecular insight into affinities of drugs and their metabolites to lipid bilayers, J. Phys. Chem. B 117 (2013) 2403–2410.
[61] H.A.L. Filipe, M.J. Moreno, T. Róg, I. Vattulainen, L.M.S. Loura, How to tackle the issues in free energy simulations of long amphiphiles interacting with lipid membranes: convergence and local membrane deformations, J. Phys. Chem. B 118 (2014) 3572–3581.
[62] R.D. Porasso, N.M. Ale, F. Ciocco Aloia, D. Masone, M.G. Del Popolo, A. Ben Altabef, A. Gomez-Zavaglia, S.B. Diaz, J.A. Vila, Interaction of glycine, lysine, proline and histidine with dipalmitoylphosphatidylcholine lipid bilayers: a theoretical and experimental study, RSC Adv. 5 (2015) 43537–43546.
[63] G.H. Peters, M. Werge, M.N. Elf-Lind, J.J. Madsen, G.F. Velardez, P. Westh, Interaction of neurotransmitters with a phospholipid bilayer: a molecular dynamics study, Chem. Phys. Lipids 184 (2014) 7–17.
[64] Y. Hu, S. Ou, S. Patel, Free energetics of arginine permeation into model DMPC lipid bilayers: coupling of effective counterion concentration and lateral bilayer dimensions, J. Phys. Chem. B 117 (2013) 11641–11653.
[65] D. Sun, J. Forsman, C.E. Woodward, Evaluating force fields for the computational prediction of ionized arginine and lysine side-chains partitioning into lipid bilayers and octanol, J. Chem. Theory Comput. 11 (2015) 1775–1791.
[66] C. Neale, C. Madill, S. Rauscher, R. Pomès, Accelerating convergence in molecular dynamics simulations of solutes in lipid membranes by conducting a random walk along the bilayer normal, J. Chem. Theory Comput. 9 (2013) 3686–3703.
[67] S. Ou, T.R. Lucas, Y. Zhong, B.A. Bauer, Y. Hu, S. Patel, Free energetics and the role of water in the permeation of methyl guanidinium across the bilayer–water interface: insights from molecular dynamics simulations using charge equilibration potentials, J. Phys. Chem. B 117 (2013) 3578–3592.
[68] L.J. Martin, R. Chao, B. Corry, Molecular dynamics simulation of the partitioning of benzocaine and phenytoin into a lipid bilayer, Biophys. Chem. 185 (2014) 98–107.
[69] J. Tian, A. Sethi, Basil I. Swanson, B. Goldstein, S. Gnanakaran, Taste of sugar at the membrane: thermodynamics and kinetics of the interaction of a disaccharide with lipid bilayers, Biophys. J. 104 (2013) 622–632.
[70] G.H. Peters, C. Wang, N. Cruys-Bagger, G.F. Velardez, J.J. Madsen, P. Westh, Binding of serotonin to lipid membranes, J. Am. Chem. Soc. 135 (2013) 2164–2171.
[71] S. Jalili, M. Saeedi, Study of curcumin behavior in two different lipid bilayer models of liposomal curcumin using molecular dynamics simulation, J. Biomol. Struct. Dyn. (2015) 1–14.
[72] M.J. Arcario, C.G. Mayne, E. Tajkhorshid, Atomistic models of general anesthetics for use in in silico biological studies, J. Phys. Chem. B 118 (2014) 12075–12086.
[73] Y. Nademi, S. Amjad Iranagh, A. Yousefpour, S. Mousavi, H. Modarress, Molecular dynamics simulations and free energy profile of paracetamol in DPPC and DMPC lipid bilayers, J. Chem. Sci. 126 (2014) 637–647.
[74] R.V. Swift, R.E. Amaro, Back to the future: can physical models of passive membrane permeability help reduce drug candidate attrition and move us beyond QSPR? Chem. Biol. Drug Des. 81 (2013) 61–71.
[75] D. Bochicchio, E. Panizon, R. Ferrando, L. Monticelli, G. Rossi, Calculating the free energy of transfer of small solutes into a model lipid membrane: comparison between metadynamics and umbrella sampling, J. Chem. Phys. 143 (2015) 144108.
[76] W. Rawicz, K.C. Olbrich, T. McIntosh, D. Needham, E. Evans, Effect of chain length and unsaturation on elasticity of lipid bilayers, Biophys. J. 79 (2000) 328–339.
[77] J.C. Mathai, S. Tristram-Nagle, J.F. Nagle, M.L. Zeidel, Structural determinants of water permeability through the lipid membrane, J. Gen. Physiol. 131 (2008) 69–76.
[78] Y. Shai, Mechanism of the binding, insertion and destabilization of phospholipid bilayer membranes by α-helical antimicrobial and cell non-selective membrane-lytic peptides, Biochim. Biophys. Acta Biomembr. 1462 (1999) 55–70.
[79] L.R. De Young, K.A. Dill, Solute partitioning into lipid bilayer membranes, Biochemistry 27 (1988) 5281–5289.
[80] R.C. Bean, W.C. Shepherd, H. Chan, Permeability of lipid bilayer membranes to organic solutes, J. Gen. Physiol. 52 (1968) 495–508.
[81] M. Jain, N. Wu, Effect of small molecules on the dipalmitoyl lecithin liposomal bilayer: III. Phase transition in lipid bilayer, J. Membr. Biol. 34 (1977) 157–201.
[82] S.-J. Marrink, H.J.C. Berendsen, Simulation of water transport through a lipid membrane, J. Phys. Chem. 98 (1994) 4155–4168.
[83] H.J.C. Berendsen, S.-J. Marrink, Molecular dynamics of water transport through membranes: water from solvent to solute, Pure Appl. Chem. 65 (1993) 2513–2520.
[84] C. Neale, W.F.D. Bennett, D.P. Tieleman, R. Pomès, Statistical convergence of equilibrium properties in simulations of molecular solutes embedded in lipid bilayers, J. Chem. Theory Comput. 7 (2011) 4175–4188.
[85] M. Orsi, J.W. Essex, Permeability of drugs and hormones through a lipid bilayer: insights from dual-resolution molecular dynamics, Soft Matter 6 (2010) 3797–3808.
[86] K. Hinsen, B. Roux, Potential of mean force and reaction rates for proton transfer in acetylacetone, J. Chem. Phys. 106 (1997) 3567–3577.
[87] L. Zheng, M. Chen, W. Yang, Random walk in orthogonal space to achieve efficient free-energy simulation of complex systems, Proc. Natl. Acad. Sci. U. S. A. 105 (2008) 20227–20232.
[88] J.L. MacCallum, W.F.D. Bennett, D.P. Tieleman, Distribution of amino acids in a lipid bilayer from computer simulations, Biophys. J. 94 (2008) 3393–3404.
[89] J.L. MacCallum, W.F.D. Bennett, D.P. Tieleman, Partitioning of amino acid side chains into lipid bilayers: results from computer simulations and comparison to experiment, J. Gen. Physiol. 129 (2007) 371–377.
[90] A.C.V. Johansson, E. Lindahl, Titratable amino acid solvation in lipid membranes as a function of protonation state, J. Phys. Chem. B 113 (2009) 245–253.
[91] S. Dorairaj, T.W. Allen, On the thermodynamic stability of a charged arginine side chain in a transmembrane helix, Proc. Natl. Acad. Sci. U. S. A. 104 (2007) 4943–4948.
[92] N. Sapay, W.F.D. Bennett, D.P. Tieleman, Thermodynamics of flip-flop and desorption for a systematic series of phosphatidylcholine lipids, Soft Matter 5 (2009) 3295–3302.
[93] W.F.D. Bennett, J.L. MacCallum, D.P. Tieleman, Thermodynamic analysis of the effect of cholesterol on dipalmitoylphosphatidylcholine lipid membranes, J. Am. Chem. Soc. 131 (2009) 1972–1978.
[94] D.P. Tieleman, S.-J. Marrink, Lipids out of equilibrium: energetics of desorption and pore mediated flip-flop, J. Am. Chem. Soc. 128 (2006) 12462–12467.
[95] A.E. Cardenas, R. Elber, Computational study of peptide permeation through membrane: searching for hidden slow variables, Mol. Phys. 111 (2013) 3565–3578.
[96] A.E. Cardenas, G.S. Jas, K.Y. DeLeon, W.A. Hegefeld, K. Kuczera, R. Elber, Unassisted transport of N-acetyl-l-tryptophanamide through membrane: experiment and simulation of kinetics, J. Phys. Chem. B 116 (2012) 2739–2750.
[97] C. Wei, A. Pohorille, Flip-flop of oleic acid in a phospholipid membrane: rate and mechanism, J. Phys. Chem. B 118 (2014) 12919–12926.
[98] C. Hofsäß, E. Lindahl, O. Edholm, Molecular dynamics simulations of phospholipid bilayers with cholesterol, Biophys. J. 84 (2003) 2192–2206.
[99] C. Neale, Jenny C.Y. Hsu, Christopher M. Yip, R. Pomès, Indolicidin binding induces thinning of a lipid bilayer, Biophys. J. 106 (2014) L29–L31.
[100] E. Darve, A. Pohorille, Calculating free energies using average force, J. Chem. Phys. 115 (2001) 9169–9183.
[101] Anthony R. Braun, Erik G. Brandt, O. Edholm, John F. Nagle, Jonathan N. Sachs, Determination of electron density profiles and area from simulations of undulating membranes, Biophys. J. 100 (2011) 2112–2120.
[102] K. Huang, A.E. García, Free energy of translocating an arginine-rich cell-penetrating peptide across a lipid bilayer suggests pore formation, Biophys. J. 104 (2013) 412–420.
[103] D.I. Kopelevich, One-dimensional potential of mean force underestimates activation barrier for transport across flexible lipid membranes, J. Chem. Phys. 139 (2013) 134906.
[104] M. Paloncýová, K. Berka, M. Otyepka, Convergence of free energy profile of coumarin in lipid bilayer, J. Chem. Theory Comput. (2012).
[105] I.-C. Yeh, D.R. Ripoll, A. Wallqvist, Free energy difference in indolicidin attraction to eukaryotic and prokaryotic model cell membranes, J. Phys. Chem. B 116 (2012) 3387–3396.
[106] D.A. Pearlman, P.A. Kollman, The lag between the Hamiltonian and the system configuration in free energy perturbation calculations, J. Chem. Phys. 91 (1989) 7831–7839.
[107] O. Berger, O. Edholm, F. Jähnig, Molecular dynamics simulations of a fluid bilayer of dipalmitoylphosphatidylcholine at full hydration, constant pressure, and constant temperature, Biophys. J. 72 (1997) 2002–2013.
[108] K. Huang, A.E. García, Effects of truncating van der Waals interactions in lipid bilayer simulations, J. Chem. Phys. 141 (2014) 105101.
[109] J.B. Klauda, R.M. Venable, J.A. Freites, J.W. O'Connor, D.J. Tobias, C. Mondragon-Ramirez, I. Vorobyov, A.D. MacKerell, R.W. Pastor, Update of the CHARMM all-atom additive force field for lipids: validation on six lipid types, J. Phys. Chem. B 114 (2010) 7830–7843.
[110] Y. Sugita, A. Kitao, Y. Okamoto, Multidimensional replica-exchange method for free-energy calculations, J. Chem. Phys. 113 (2000) 6042–6051.

[111] S. Rauscher, C. Neale, R. Pomès, Simulated tempering distributed replica sampling, virtual replica exchange, and other generalized-ensemble methods for conformational sampling, J. Chem. Theory Comput. 5 (2009) 2640–2662.
[112] L. Sutto, S. Marsili, F.L. Gervasio, New advances in metadynamics, Wiley Interdiscip. Rev. Comput. Mol. Sci. 2 (2012) 771–779.
[113] J. Hénin, G. Fiorin, C. Chipot, M.L. Klein, Exploring multidimensional free energy landscapes using time-dependent biases on collective variables, J. Chem. Theory Comput. 6 (2010) 35–47.
[114] S.A. Paz, C.F. Abrams, Free energy and hidden barriers of the β-sheet structure of prion protein, J. Chem. Theory Comput. 11 (2015) 5024–5034.
[115] M.J. Hinner, S.-J. Marrink, A.H. de Vries, Location, tilt, and binding: a molecular dynamics study of voltage-sensitive dyes in biomembranes, J. Phys. Chem. B 113 (2009) 15807–15819.
[116] W.F.D. Bennett, D.P. Tieleman, Water defect and pore formation in atomistic and coarse-grained lipid membranes: pushing the limits of coarse graining, J. Chem. Theory Comput. 7 (2011) 2981–2988.
[117] Y. Mao, Y. Du, X. Cang, J. Wang, Z. Chen, H. Yang, H. Jiang, Binding competition to the POPG lipid bilayer of Ca2+, Mg2+, Na+, and K+ in different ion mixtures and biological implication, J. Phys. Chem. B 117 (2013) 850–858.
[118] D. Lin, A. Grossfield, Thermodynamics of micelle formation and membrane fusion modulate antimicrobial lipopeptide activity, Biophys. J. 109 (2015) 750–759.
[119] Z. Ghaemi, M. Minozzi, P. Carloni, A. Laio, A novel approach to the investigation of passive molecular permeation through lipid bilayers from atomistic simulations, J. Phys. Chem. B 116 (2012) 8714–8721.
[120] D. Bemporad, J.W. Essex, C. Luttmann, Permeation of small molecules through a lipid bilayer: a computer simulation study, J. Phys. Chem. B 108 (2004) 4875–4884.
[121] J.L. MacCallum, W.F.D. Bennett, D.P. Tieleman, Transfer of arginine into lipid bilayers is nonadditive, Biophys. J. 101 (2011) 110–117.